Mon. Not. R. Astron. Soc. **393,** 846–857 (2009) doi:10.1111/j.1365-2966.2008.13969.x

The CaT strength in Seyfert nuclei revisited: analysing young stars and non-stellar light contributions to the spectra

L. R. Vega,[1,2⋆] N. V. Asari,[3⋆] R. Cid Fernandes,[3⋆] A. Garcia-Rissmann,[4⋆] T. Storchi-Bergmann,[5⋆] R. M. González Delgado[6⋆] and H. Schmitt[7,8⋆]

[1]*Instituto de Astronomía Teórica y Experimental, IATE - Observatorio Astronómico, Universidad Nacional de Córdoba Laprida 854, X5000BGR Córdoba, Argentina*
[2]*Secyt, Secretaría de Ciencia y Técnica de la Universidad Nacional de Córdoba, Córdoba, Argentina*
[3]*Universidade Federal de Santa Catarina, Florianópolis, Brazil*
[4]*European Southern Observatory, Karl-Schwarzschild Str 2, D-85748 Garching b. München, Germany*
[5]*Instituto de Física, Universidade Federal do Rio Grande do Sul, C.P. 15001, 91501-970, Porto Alegre, RS, Brazil*
[6]*Instituto de Astrofísica de Andalucía (CSIC), PO Box 3004, 18080 Granada, Spain*
[7]*Remote Sensing Division, Naval Research Laboratory, Washington, DC 20375, USA*
[8]*Interferometrics, Inc., Herdon, VA 20171, USA*

Accepted 2008 September 15. Received 2008 September 15; in original form 2007 December

ABSTRACT

In a former paper, we have presented spectra of 64 active, nine normal and five starburst galaxies in the region around the near-infrared calcium triplet (CaT) absorption lines and the [S III]λ9069 line. In the present paper, we analyse the CaT strength ($W_{\rm CaT}$) and kinematical products derived in that study, namely stellar ($\sigma_\star$) and ionized gas ($\sigma_{\rm gas}$) velocity dispersions. Our main results may be summarized as follows. (1) Type 2 Seyfert galaxies show no sign of dilution in $W_{\rm CaT}$ with respect to the values spanned by normal galaxies, even when optical absorption lines such as the Ca II *K* band at 3933 Å are much weaker than in old, bulge-like stellar populations. (2) The location of type 2 Seyfert galaxies in the $W_{\rm CaT}$–$W_{\rm CaK}$ plane is consistent with evolutionary synthesis models. The implication is that the source responsible for the dilution of optical lines in these active galactic nuclei (AGN) is a young stellar population, rather than an AGN featureless continuum, confirming the conclusion of the pioneer study of Terlevich, Díaz & Terlevich. (3) In type 1 Seyfert galaxies, both $W_{\rm [S\,III]}$ and $W_{\rm CaT}$ tend to be diluted due to the presence of a non-stellar component, in agreement with the unification paradigm. (4) A comparison of $\sigma_\star$ with $\sigma_{\rm gas}$ (obtained from the *core* of the [S III] emitting line) confirms the existence of a correlation between the typical velocities of stars and clouds of the narrow line region. The strength and scatter around this correlation are similar to those previously obtained from the [O III]λ5007 linewidth.

Key words: galaxies: kinematics and dynamics – galaxies: nuclei – galaxies: Seyfert – galaxies: stellar content.

1 INTRODUCTION

The stellar absorption lines from the near-infrared (IR) calcium triplet (CaT) made their debut in the field of active galactic nuclei (AGN) with the work of Terlevich, Díaz & Terlevich (1990, hereafter TDT). At that time, it was thought that the optical spectrum of type 2 Seyfert galaxies contained a featureless continuum (FC) from the AGN, which, in light of unification scenarios (Antonucci 1993), should be associated with scattered light from the hidden Seyfert 1 nucleus (Cid Fernandes & Terlevich 1995). TDT realized that this idea could not be fully correct, since their data indicated that, unlike for absorption lines in the optical, the strength of the CaT in these sources shows no signs of dilution with respect to the values found in normal galaxies. Their interpretation of this fact was that what was called a 'non-stellar FC' was in fact a stellar component associated to young stellar populations. This conclusion was thoroughly confirmed by numerous studies in the past decade (see Cid Fernandes et al. 2004 for a review).

Since then, interest in the CaT shifted towards its use as a tracer of stellar kinematics, particularly in AGN. The location of the CaT in a relatively clean spectral region makes it an ideal feature to measure stellar velocity dispersions ($\sigma_\star$), which trace the gravitational potential of the host galaxy's bulge. In an influential work, Nelson

⋆E-mail: luisv@mail.oac.uncor.edu (LRV); natalia@astro.ufsc.br (NVA); cid@astro.ufsc.br (RCF); agarciar@eso.org (AGR); thaisa@if.ufrgs.br (TSB); rosa@iaa.es (RMGD); henrique.schmitt@nrl.navy.mil (HS)

& Whittle (1996, hereafter NW) used the CaT in a comparison between stellar and gaseous kinematics of AGN, finding that the typical velocity narrow line region (NLR) clouds ($\sigma_{\rm gas}$) correlate with $\sigma_\star$, albeit with a significant scatter. More recently, a strong correlation between $\sigma_\star$ and black hole mass (Tremaine et al. 2002 and references therein) indirectly boosted interest in observations of the CaT (Nelson 2000; Botte et al. 2004).

For completely different reasons, recent work on normal galaxies has also raised the interest in the CaT. Empirical investigations have revealed rather puzzling behaviour of the CaT in bulges and elliptical galaxies. First, detailed population synthesis models tend to overpredict the CaT strength (Saglia et al. 2002; Cenarro et al. 2003, 2004), particularly for giant ellipticals, though for dwarf ellipticals the match between data and models is satisfactory (Michielsen et al. 2007). Secondly, while classic metallicity tracers like the Mg_2 index are known to correlate with $\sigma_\star$ (e.g. Terlevich et al. 1981), tracing the well-known mass–metallicity relation, the strength of the CaT appears to be *anti-correlated* with $\sigma_\star$ (Cenarro et al. 2003, 2004; Falcón-Barroso et al. 2003; Michielsen et al. 2003). The interpretation of these results is still not clear, and the situation is likely to be even more complex in systems with varied star formation histories like AGN (Cid Fernandes et al. 2004; Wild et al. 2007).

One thus sees that, more than 15 years after TDT introduced the CaT in AGN research, there are still plenty of reasons to keep studying it. With this general motivation, in Garcia-Rissmann et al. (2005) (hereafter Paper I) we have carried out a spectroscopic survey of Seyfert galaxies in the region including the CaT and the [S III]λ9069 emission line. Paper I concentrated on the presentation of the data and the derivation of four main data products: stellar velocity dispersions ($\sigma_\star$), [S III] emission linewidths ($\sigma_{\rm [S\,III]}$, which is representative of the highly ionized component of the gas of the NLR in AGN), [S III] equivalent widths ($W_{\rm [S\,III]}$) and the CaT strength ($W_{\rm CaT}$). Here, we use these data to address the following issues. (1) Examine the contribution of a non-stellar component in the near-IR spectra of Seyfert galaxies and test the consistency of $W_{\rm [S\,III]}$ and $W_{\rm CaT}$ data with the unified model; (2) study the sensitivity of $W_{\rm CaT}$ to stellar population properties; (3) investigate the connection between NLR and stellar kinematics and CaT strength and (4) report results of spatially resolved spectroscopy, not reported in Paper I.

To study these questions, we complement the data in Paper I with values of the equivalent width of the Ca II K line ($W_{\rm CaK}$) obtained from previous studies. As shown by Cid Fernandes et al. (2001), the Ca II K line is a powerful tracer of stellar populations even in type 2 Seyferts. By comparing $W_{\rm CaT}$ with $W_{\rm CaK}$, we can assess whether the CaT is a useful stellar population tracer, and determine whether the combination of CaK and CaT strengths is explained as due to stars alone or if a FC component is necessary. We also add in literature information on the width ($\sigma_{\rm [O\,III]}$) of the [O III]λ5007 line, which is useful to test whether our results are somehow affected by the choice of [S III]λ9069 as a tracer of NLR motions.

This paper is organized as follows. Section 2 presents a series of studies related to the CaT strength. After showing CaT observational properties in Section 2.1, we compare $W_{\rm CaT}$ with $W_{\rm CaK}$ in Section 2.2 and investigate whether the location of the points in the $W_{\rm CaT}$ versus $W_{\rm CaK}$ diagram is consistent with the existence of a FC at near-IR wavelengths. In Section 3, we use evolutionary synthesis models to track the behaviour of both $W_{\rm CaT}$ and $W_{\rm CaK}$ as a function of age and metallicity, and overlay the models on to the data in the $W_{\rm CaT}$ versus $W_{\rm CaK}$ diagram. In Section 4, we study the spatial behaviour of $\sigma_\star$ and $W_{\rm CaT}$ for about half of our sample. In Section 5, we analyse stellar and ionized gas kinematics: stellar velocity dispersions and its relation to CaT are studied in Section 5.1, while in Section 5.2 we discuss the link between stellar and gas kinematics. Finally, Section 6 summarizes our main results.

2 THE CAT STRENGTH: EFFECTS OF NON-STELLAR LIGHT

One of our goals is to evaluate the usefulness of the CaT as a stellar population diagnostic. Since our sample is dominated by AGN, before discussing stellar populations we must first examine to which extent non-stellar light affects our CaT measurements.

As explained in Paper I, we adopt the $W_{\rm CaT}$ and $W_{\rm CaT*}$ definitions of Cenarro et al. (2001a). They offer two definitions of the CaT equivalent width: 'CaT' (which we call $W_{\rm CaT}$), which consists of a sum of the equivalent widths of all three CaT lines, and 'CaT*' (called $W_{\rm CaT*}$ here), which corrects $W_{\rm CaT}$ for contamination by Paschen line absorption. These equivalent widths are measured with respect to a continuum defined by fitting the spectrum in five windows in the 8474–8792 Å range. Because of the presence of unwanted features in the observed spectra, we opted to measure $W_{\rm CaT}$ and $W_{\rm CaT*}$ on the synthetic spectra. On the other hand, our spectral base used to fit the observed spectra does not have stars with the spectral types with Paschen lines, so we use $W_{\rm CaT}$ as equivalent width measurements for our spectra.

All nuclear CaT data refer to apertures of $\sim 2 \times 2$ arcsec^2 (Paper I). To take into account the different velocity dispersions of our galaxies, we broadened each spectrum to match the largest value of ${\sigma_\star}^2 + {\sigma_{\rm inst}}^2$ of our sample, corresponding to NGC 3115 ($\sigma_\star = 275$ and $\sigma_{\rm inst} = 56\,{\rm km\,s^{-1}}$). This correction changes the value of $W_{\rm CaT}$ by typically 10 per cent with respect to the uncorrected values given in Paper I. $W_{\rm CaK}$ measurements from Cid Fernandes et al. (2004) are also used in our analysis.

2.1 Seyfert 1s x Seyfert 2s

It is well known that a non-stellar light is present in type 1 Seyfert galaxies. The contribution of such a component in type 2 Seyfert galaxies has been a topic of much controversy in the past. One way to address this issue is to compare type 1 Seyfert galaxies with type 2 Seyfert galaxies through CaT.

Fig. 1 (top panel) shows the distributions of $W_{\rm CaT}$ for Seyfert galaxies in our sample, with type 1 Seyfert galaxies (including subtypes 1–1.9) marked by the filled areas. Almost all type 2 Seyfert galaxies lie between 4 and 8 Å, with a median of 6.5 Å. $W_{\rm CaT}$ tends to be smaller in type 1 nuclei, with a median of 4.8 Å. Emission lines from the NLR follow the same pattern, with smaller equivalent widths in Seyfert 1s than in type 2 Seyfert galaxies, as shown for [S III]λ9069 in the bottom panel of Fig. 1.

Another way of illustrating this result is shown in Fig. 2, where we plot the CaT strength as a function of the fractional contribution of power laws to the continuum in the CaT region. This fraction, which we denote as $x_{\rm PL}$, is deduced from the spectral fits presented in Paper I, where, besides observed stars, power laws of several slopes were included to emulate the effects of a template mismatch in the $\sigma_\star$ measurements. Table 1 lists $x_{\rm PL}$, along with the new (corrected) $W_{\rm CaT}$ values mentioned at the beginning of this section and their errors.

The plot shows that $x_{\rm PL}$ is smaller for type 2 Seyfert galaxies than for type 1 Seyfert galaxies. Furthermore, the values of both $x_{\rm PL}$ and $W_{\rm CaT}$ obtained for type 2 Seyfert galaxies span approximately the same range as those found for the non-active galaxies in the sample.

The fact that $W_{\rm CaT}$(Sey1) < $W_{\rm CaT}$(Sey2) and similarly $W_{\rm [S\,III]}$ (Sey 1) < $W_{\rm [S\,III]}$(Sey 2) is consistent with the unified model, which

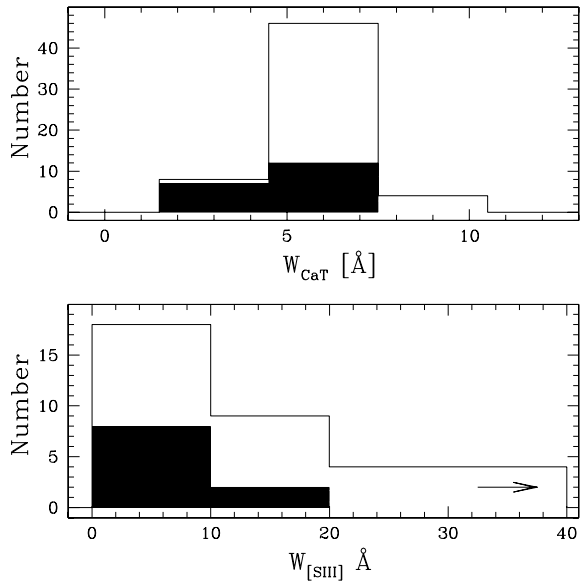

Figure 1. Distributions of the equivalent width of the CaT absorption lines (top) and of the [S III]λ9069 emission line (bottom) for Seyfert 1 (filled areas) and Seyfert 2 (empty areas).

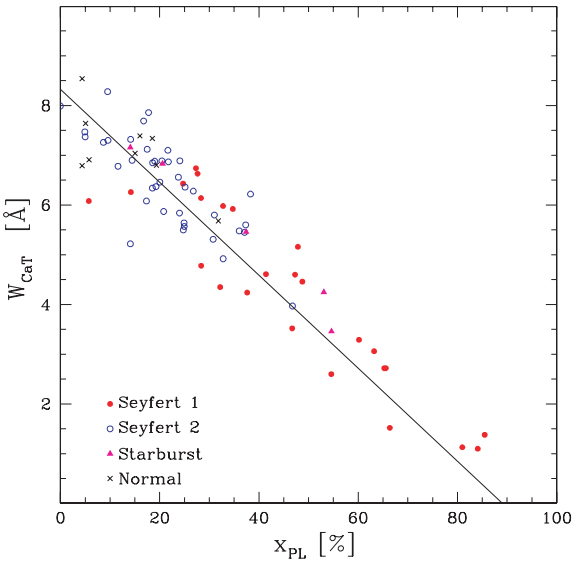

Figure 2. $W_{\rm CaT}$ versus percentage of power-law contribution to the synthesis. Hereafter, symbols are like in this figure.

predicts a dilution of the equivalent widths of the absorption and emission lines in sources where the nuclear non-stellar continuum is seen directly. The fact that the range of CaT strengths spanned by type 2 Seyfert galaxies is similar to that spanned by non-active galaxies indicates that their scattered FC, if present, is too weak to produce a notable effect on the near-IR range.

2.2 Dilution by an underlying FC: the CaT versus CaK diagram

While the results reported above suggest that one does not need to worry about non-stellar light in the CaT range in type 2 Seyfert galaxies, it is desirable to test this idea more conclusively before proceeding to an analysis of $W_{\rm CaT}$ in terms of stellar populations alone. This can be done combining our CaT data with information from a different wavelength range. The equivalent width of the Ca II K absorption at 3933 Å ($W_{\rm CaK}$) provides the necessary information.

The CaK line, which originates in old, late-type stars from the host's bulge, is very sensitive to dilution by an underlying blue continuum. As usual, this continuum can be due to either an AGN or a young stellar population, and the value of $W_{\rm CaK}$ by itself cannot distinguish between these two possibilities (e.g. Storchi-Bergmann et al. 2000). The combination of $W_{\rm CaK}$ and $W_{\rm CaT}$ data helps lifting this ambiguity.

The idea, first developed by TDT, is simple: if the CaK is diluted by a truly FC, and if this FC extends from the optical to the near-IR, then the CaT would be diluted too, and by a predictable amount. From observations of type 1 Seyferts and quasars, we know that the AGN optical continuum is well described by a power-law $F_\nu^{\rm FC} \propto \nu^{-\alpha}$, with α in the 1–2 range or, equivalently, $F_\lambda^{\rm FC} \propto \lambda^{-\beta}$, with $\beta = 2 - \alpha$. This FC is superposed to the bulge stellar light.

Suppose that the bulge has intrinsic CaK and CaT equivalent widths $W^\star_{\rm CaK}$ and $W^\star_{\rm CaT}$, and that the ratio of the stellar continuum fluxes over these two lines is $c^\star \equiv C^\star_{\lambda_{\rm CaK}}/C^\star_{\lambda_{\rm CaT}}$. Trivial algebra then leads to the following relation between the observed CaK and CaT equivalent widths:

$$W_{\rm CaK} = W^*_{\rm CaK}\left(1 - x^{\rm FC}_{\rm CaK}\right). \quad (1)$$

$$W_{\rm CaT} = W^*_{\rm CaT}\frac{1}{1 + c^\star \times \left(\frac{\lambda_{\rm CaT}}{\lambda_{\rm CaK}}\right)^{-\beta} \times \frac{x^{\rm FC}_{\rm CaK}}{1-x^{\rm FC}_{\rm CaK}}}, \quad (2)$$

where $x^{\rm FC}_{\rm CaK}$ is the fraction of the total continuum at 3933 Å which comes from the FC.

We modelled a mixing of a FC and bulge continuum in a form of 'FC + SSP' mixing lines, where SSP refers to a Simple Stellar Population representative of 10 Gyr old, typical of elliptical galaxies and bulges, as obtained from Bruzual & Charlot (2003, hereafter BC03) models for solar metallicity. Practical use of equation (2) requires stipulating fiducial values for $W^\star_{\rm CaK}$, $W^\star_{\rm CaT}$ and $c^\star$. We adopt $(W^\star_{\rm CaK}, W^\star_{\rm CaT}) = (21.1, 7.9)$ Å and $c^\star = 0.38$.

Equation (2) is overplotted to the data points in the $W_{\rm CaT}$ versus $W_{\rm CaK}$ diagram (Fig. 3). The lines indicate the bulge + FC mixing lines for different values of the slope α and for $x^{\rm FC}_{\rm CaK}$ decreasing from 100 per cent at $(W_{\rm CaT}, W_{\rm CaK}) = (0, 0)$ to 0 per cent at $(W_{\rm CaT}, W_{\rm CaK}) = (W^\star_{\rm CaT}, W^\star_{\rm CaK})$. The $W_{\rm CaK}$ measurements come from the optical studies of Cid Fernandes, Storchi-Bergmann & Schmitt (1998) and Cid Fernandes et al. (2001, 2004). Of the 78 galaxies in our sample, 42 overlap with these studies, most of which (31) correspond to type 2 Seyfert galaxies.

We see that some Seyfert nuclei line up along the mixing lines. However, in order to explain all of the objects, it is necessary a contribution of $x^{\rm FC}_{\rm CaK}$ of about 50 per cent or greater. There are some Seyfert with high $W_{\rm CaT}$ and low $W_{\rm CaK}$ that are not explained in terms of these mixing lines for α between 1 ($\beta = 1$) and 2 ($\beta = 0$), which are representative of type 1 AGN. For these objects, only if α were as low as ∼0.5 or less the dilution lines would go approximately through the observed values, but not even quasars have such an extremely blue continuum. Such a blue FC could in principle be produced by scattering of the AGN light by dust particles. Nevertheless, the required values of the $x^{\rm FC}_{\rm CaK}$ fraction (of the order of ∼50 per cent) would imply that scattered broad lines in the optical should become visible, in which case the galaxy would not be classified as a type 2 Seyfert galaxy in the first place (an argument first put forward by Cid Fernandes & Terlevich 1995). Besides that, about half of the type 2 Seyfert galaxies with $x^{\rm FC}_{\rm CaK}$ greater than

Table 1. Results of W_{CaT} and x_{PL}. Columns list galaxy name, type of activity, W_{CaT} and x_{PL} contribution. All W_{CaT} data are measured in the same system, as explained in the text.

Name	Type	W_{CaT} (Å)	x_{PL} (per cent)	Name	Type	W_{CaT} (Å)	x_{PL} (per cent)
NGC 205	Normal	5.68 ± 0.46	32	NGC 7410	Sy 2	7.10 ± 0.46	22
NGC 526A	Sy 1.9	4.46 ± 0.45	49	NGC 7469	Sy 1.5	2.72 ± 0.45	65
NGC 526B	Normal	6.80 ± 0.47	19	NGC 7496	Sy 2	5.45 ± 0.47	37
NGC 1019	Sy 1.5	5.92 ± 0.44	35	NGC 7582	Sy 2	5.22 ± 0.47	14
NGC 1068	Sy 2	5.84 ± 0.48	24	NGC 7590	Sy 2	7.12 ± 0.43	17
NGC 1125	Sy 2	6.89 ± 0.46	21	NGC 7714	Sy 3	4.25 ± 0.46	53
NGC 1140	Starburst	5.46 ± 0.44	37	MARK 0001	Sy 2	5.64 ± 0.46	25
NGC 1142	Sy 2	7.99 ± 0.46	0	MARK 0003	Sy 2	3.97 ± 0.48	47
NGC 1241	Sy 2	7.86 ± 0.43	18	MARK 0040	Sy 1	4.24 ± 0.46	38
NGC 1365	Sy 1.8	0.93 ± 0.46	85	MARK 0078	Sy 2	6.90 ± 0.45	15
NGC 1380	Normal	7.64 ± 0.46	5	MARK 0079	Sy 1.2	2.64 ± 0.46	55
NGC 1386	Sy 2	7.47 ± 0.46	5	MARK 0273	Sy 2	7.30 ± 0.44	10
NGC 1433	Normal	6.79 ± 0.44	4	MARK 0348	Sy 2	5.87 ± 0.44	21
NGC 1672	Starburst	7.16 ± 0.44	14	MARK 0372	Sy 1.5	6.08 ± 0.46	6
NGC 1808	Starburst	6.83 ± 0.46	21	MARK 0461	Sy 2	5.57 ± 0.46	25
NGC 2110	Sy 2	6.34 ± 0.47	19	MARK 0516	Sy 1.8	6.63 ± 0.46	28
NGC 2639	Sy 1.9	6.74 ± 0.44	27	MARK 0573	Sy 2	7.26 ± 0.44	9
NGC 2997	Normal	7.39 ± 0.45	16	MARK 0705	Sy 1.2	4.61 ± 0.46	41
NGC 3081	Sy 2	6.89 ± 0.46	24	MARK 0915	Sy 1.8	4.78 ± 0.47	28
NGC 3115	Normal	7.04 ± 0.45	15	MARK 1066	Sy 2	5.31 ± 0.45	31
NGC 3256	Starburst	3.46 ± 0.46	55	MARK 1073	Sy 2	5.50 ± 0.46	25
NGC 3281	Sy 2	6.85 ± 0.45	19	MARK 1210	Sy 2	6.22 ± 0.48	38
NGC 3783	Sy 1.5	2.72 ± 0.45	66	MARK 1239	Sy 1.5	0.92 ± 0.47	81
NGC 4339	Normal	6.91 ± 0.46	6	ESO 362-G08	Sy 2	6.87 ± 0.45	22
NGC 4507	Sy 2	6.56 ± 0.45	24	ESO 362-G18	Sy 1.5	6.14 ± 0.45	28
NGC 4593	Sy 1	3.29 ± 0.45	60	IC 2560	Sy 2	7.32 ± 0.45	14
NGC 4748	Sy 1	3.06 ± 0.44	63	IC 3639	Sy 2	5.80 ± 0.46	31
NGC 4968	Sy 2	6.46 ± 0.45	20	IC 5169	Sy 2	6.88 ± 0.45	19
NGC 5135	Sy 2	5.60 ± 0.46	37	IRAS 01475−0740	Sy 2	5.48 ± 0.47	36
NGC 5929	Sy 2	6.08 ± 0.46	17	IRAS 04502−0317	Sy 2	6.37 ± 0.47	19
NGC 6300	Sy 2	7.69 ± 0.44	17	MCG −01-24-012	Sy 2	6.28 ± 0.47	27
NGC 6814	Sy 1.5	3.52 ± 0.47	47	MCG −02-08-039	Sy 2	7.37 ± 0.46	5
NGC 6860	Sy 1.5	5.16 ± 0.43	48	MCG −06-30-015	Sy 1.5	4.60 ± 0.45	47
NGC 6907	Normal	8.54 ± 0.44	4	MCG +8-11-11	Sy 1.5	0.92 ± 0.44	84
NGC 6951	Sy 2	8.28 ± 0.45	10	UGC 1395	Sy 1.9	5.98 ± 0.45	33
NGC 7130	Sy 1.9	6.43 ± 0.45	25	UGC 12138	Sy 1.8	6.26 ± 0.44	14
NGC 7172	Sy 2	6.36 ± 0.44	25	UGC 12348	Sy 2	6.78 ± 0.45	12
NGC 7184	Normal	7.34 ± 0.44	19	UGC 3478	Sy 1.2	1.28 ± 0.44	66
NGC 7212	Sy 2	4.92 ± 0.46	33	AKN 564	Sy 1.8	3.05 ± 0.49	32

50 per cent show high-order Balmer lines (HOBL) in absorption in their spectra (González Delgado, Heckman & Leitherer 2001). So, undiluted HOBL argue against a dilution by a power law in these objects.

We have to point out that 'FC + SSP' in Fig. 3 are computed with a solar SSP values. For another metallicities, fiducial numbers are a little different (mainly lower W_{CaT}), and the lines would go down for about 1 Å. In that way, mixing lines in Fig. 3 should be considered as an upper limit for 'FC + SSP' models.

We also computed 'FC + E' models (not shown in Fig. 3), where E refers to NGC 2110, the earliest ($t = -3$) type 2 Seyfert Galaxy in our sample for which we have determined W_{CaK} and W_{CaT}. For this model, $(W^{\star}_{CaK}, W^{\star}_{CaT}) = (13.5, 6.34)$ Å and the dilution lines would stay even more distant from the data for the same range of α considered before. So, our main conclusions about FC + bulge mixing models for Seyfert 2 nuclei remain valid.

TDT have performed the same analysis, but using the Mg_1b line at 5175 Å instead of CaK (see also Jiménez-Benito et al. 2000). They conclude that if the observed dilution of MgIb is due to a power-law FC of reasonable slope, then the CaT would also be diluted, contrary to their empirical result. Here, we considered 'FC + SSP' mixing models with some reasonable combination of $W^{\star}_{CaK}$, $W^{\star}_{CaT}$ and $c^{\star}$ values representative of old stellar populations. These models show that the dilution by a power-law FC seems to be not completely adequate to account for the observed strengths of optical and near-IR ranges simultaneously. Hence, a simple mixture of a bulge-like component plus an AGN-like FC, envisaged in the early days of AGN research (e.g. Koski 1978), is just not a viable description of the data. We will analyse another explanation for W_{CaK} and W_{CaT} behaviour in the next section.

3 CAT STRENGTH AS A STELLAR POPULATION DIAGNOSTIC

Now that we considered dilution by non-stellar light in the CaT range in type 2 Seyfert galaxies, we will proceed to a stellar population analysis.

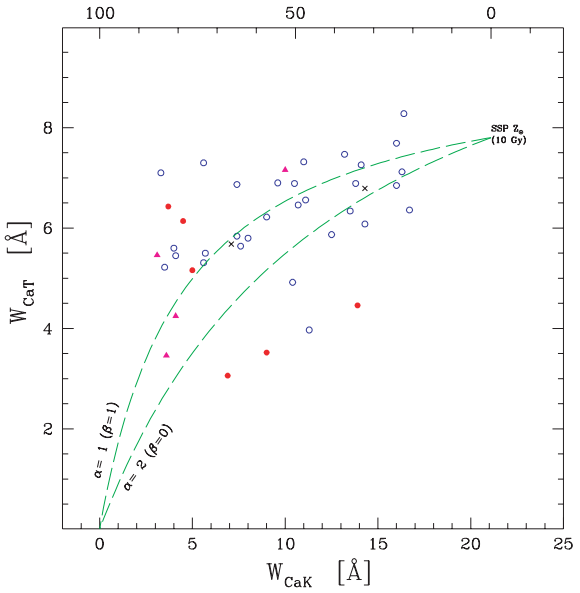

Figure 3. Equivalent width of the CaT (from Paper I) plotted against the equivalent width of the Ca II K line (from the literature). The lines show the expected dilution curves (equation 2) for bulge plus FC power laws, with slopes $\alpha = 1$ and 2 (typical range of type 1 AGN), as labelled. Upper scale shows the percentage of $x^{\rm FC}_{\rm CaK}$ contribution. Symbols are as in Fig. 2.

The behaviour of the CaT equivalent width as a function of stellar parameters ($T_{\rm eff}$, log g, [Fe/H]) has been addressed by several studies (e.g. Díaz, Terlevich & Terlevich 1989), and this knowledge has been incorporated into population synthesis models which map the CaT dependence on the age and metallicity of coeval stellar populations (e.g. Idiart, Thevenin & de Freitas Pacheco 1997). In a recent and comprehensive study, Cenarro and co-workers revisited this topic, analysing the CaT in a large library of stars and producing state-of-the-art predictions for the behaviour of the CaT in integrated stellar populations (Cenarro et al. 2001a,b, 2002; Vazdekis et al. 2003).

Despite early hopes that the CaT could serve as a metallicity indicator for galaxies (as it does for globular clusters, at least below $\sim$0.3 $Z_\odot$; Armandroff & Zinn 1988; Idiart et al. 1997; Vazdekis et al. 2003), or as tracers of recent star formation through its sensitivity to the presence of red super-giants (RSG; see TDT; Mayya 1997; García-Vargas, Molla & Bressan 1998), observations have revealed that the CaT shows remarkably little variation in strength for galaxies spanning wide ranges in morphological and stellar population properties. This small sensitivity is qualitatively consistent with the new generation of synthesis models (Vazdekis et al. 2003), which show that, for metallicities higher than ~ -0.5 dex, this feature varies little as a function of age and metallicity.

Overall, these results raise serious doubts as to the usefulness of the CaT as a stellar population diagnostic. In this section, we take another look at this issue, tackling it from an empirical perspective. As in the previous section, information on the CaK line will be incorporated in the analysis.

3.1 CaT versus CaK

Let us assume that strongly diluted CaK lines in type 2 Seyfert galaxies are the result of the presence of a starburst component, in line with previous investigations. In particular, Cid Fernandes et al. (2001) propose that type 2 Seyfert galaxies with $W_{\rm CaK} \leq 10$ Å can be safely identified as composite starburst + AGN systems, where the starburst is unambiguously identified by independent features such as the Wolf–Rayet (WR) bump or P Cygni line profiles in the ultraviolet. Investigating the behaviour of $W_{\rm CaT}$ as a function of $W_{\rm CaK}$ thus provides a fully empirical test of whether the CaT is or is not sensitive to stellar populations.

A CaT versus CaK diagram was already shown in Fig. 3, where most points correspond to type 2 Seyfert galaxies. The plot shows that $W_{\rm CaT}$ bears little, if any, relation to $W_{\rm CaK}$. It is therefore hard to evade the conclusion that for the mean ages and metallicities of metal-rich stellar populations, $W_{\rm CaT}$ is a poor diagnostic: objects as diverse as Mrk 1210, which contains a powerful young starburst, including WR stars (Storchi-Bergmann, Cid Fernandes & Schmitt 1998), and NGC 7172, which is dominated by $\sim$10 Gyr stars (Cid Fernandes et al. 2004), have $W_{\rm CaT}$ values indistinguishable within the errors (6.7 $\pm$ 0.4 and 6.9 $\pm$ 1.1 Å, respectively).

In Fig. 4, we combine our CaT data with the results of the detailed spectral synthesis analysis of type 2 Seyfert galaxies carried out by Cid Fernandes et al. (2004) for 14 sources in common with our sample. We compare their young stars (age <25 Myr) plus 'FC' light fractions at 4020 Å ($x_{Y/\rm FC}$) with both $W_{\rm CaT}$ (left-hand panel) and $W_{\rm CaK}$ (right-hand panel). As discussed in that paper, which dealt exclusively with spectra in the 3500–5200 Å range, what the synthesis returns as a FC is in most cases a reddened starburst component instead of a true non-stellar component, such that $x_{Y/\rm FC}$ is in practice a measure of the starburst strength.

The near constancy of $W_{\rm CaT}$, already evident in Fig. 3, is even more striking in Fig. 4. The inexistent correlation between CaT strength and $x_{Y/\rm FC}$ contrasts with the strong decrease in $W_{\rm CaK}$ as the starburst component increases in strength. Again, one is led to the conclusion that, by itself, $W_{\rm CaT}$ is not a stellar population tracer for our galaxies.

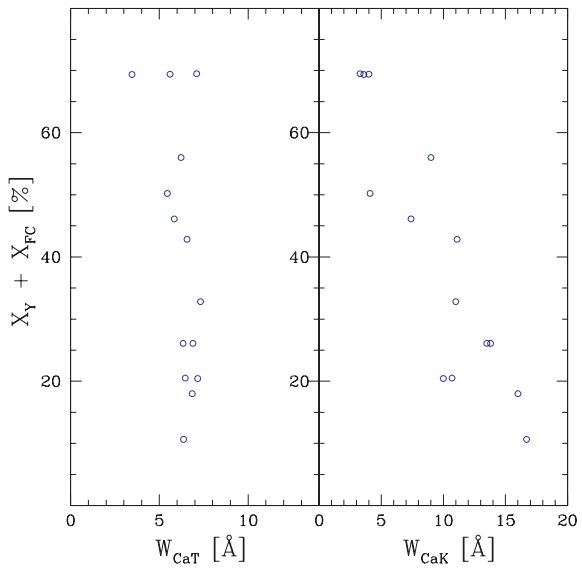

Figure 4. Percentage of a starburst component (see text) contribution to the light in synthetic spectra versus $W_{\rm CaT}$ (left-hand panel) and $W_{\rm CaK}$ (right-hand panel) in type 2 Seyfert galaxies. Note the contrast of the behaviour of $W_{\rm CaK}$, which is very sensitive to young stars, with the approximate constancy of $W_{\rm CaT}$.

3.2 Evolutionary synthesis models in the CaT versus CaK plane

The most natural interpretation of Figs 3 and 4 is that the dilution of optical lines in some Seyfert 2 nuclei is due to a young stellar population which causes little or no dilution of the CaT. In this section, we use models to check whether this is a viable scenario.

To investigate the behaviour of the CaT and CaK lines as a function of stellar population properties, we have computed the evolution of $W_{\rm CaT}$ and $W_{\rm CaK}$ for SSP for four metallicities. BC03 evolutionary synthesis models were used for this purpose. SSP models are computed with the STELIB library (Le Borgne et al. 2003), Chabrier (2003) mass function and Padova 1994 tracks (see BC03 for details). Because $W_{\rm CaT}$, $W_{\rm CaT*}$ and $W_{\rm CaK}$ are not provided in the standard BC03 distribution, they were computed directly from the theoretical spectral energy distributions, as explained at the beginning of Section 2. For compatibility with our $W_{\rm CaT}$ measurements, we broadened all model spectra as explained at the beginning of Section 2, adopting for the instrumental resolution that of the STELIB library ($\sim$45 km s^{-1} at $\sim$8600 Å).

Fig. 5 shows the results for four different metallicities: 0.2, 0.4, 1 and 2.5 $Z_\odot$. $W_{\rm CaK}$ is practically null during the first $\sim 10^{8.5}$ yr. After these initial phases, the CaK strength increases monotonically with time, which makes it good to discriminate very young SSP (younger than $\sim 3 \times 10^8$ yr) from SSP older than $\sim$1 Gyr. On the other hand, $W_{\rm CaT}$ starts from small values up to a few Myr, when the first RSG appear. The exact timing and duration of this phase depend on the metallicity. From $\sim$10 Myr to about 1 Gyr, $W_{\rm CaT}$ varies between 6 Å and 8 Å as long as RSG are replaced by red giants. Throughout these different phases, however, $W_{\rm CaT}$ spans a small range, from $\sim$6 to 8 Å. Taking into account the uncertainties in both models and data, this is in practice a constant value. Only in the first Myr of evolution does $W_{\rm CaT}$ have a useful diagnostic power, as it assumes much smaller values. Note that in these early phases, $W_{\rm CaT}$ is contaminated by Paschen lines, which explains why it does not start from 0 at $t = 0$.

In Fig. 6, these models are overlaid to the data in the $W_{\rm CaT}$ versus $W_{\rm CaK}$ diagram. Type 1 Seyfert galaxies are not plotted because of their non-stellar continuum, which affects both CaK and CaT.

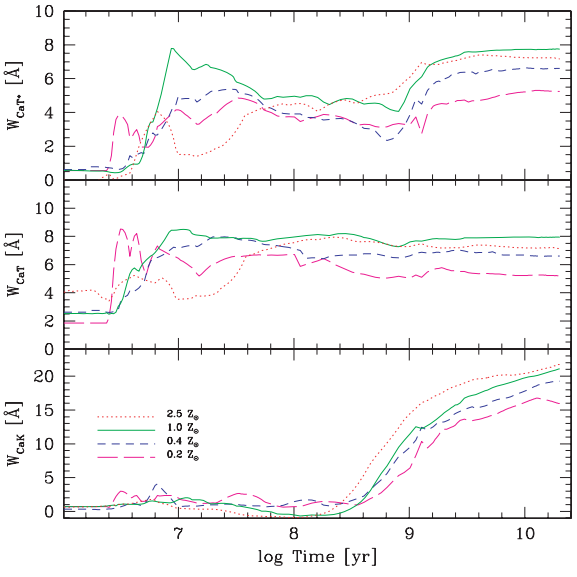

Figure 5. Evolution of the $W_{\rm CaT*}$, $W_{\rm CaT}$ and $W_{\rm CaK}$ absorption line indices for SSP, from BC03 models. Long dashed, dashed, solid and dotted lines correspond to metallicities of 0.2, 0.4, 1 and 2.5 $Z_\odot$, respectively.

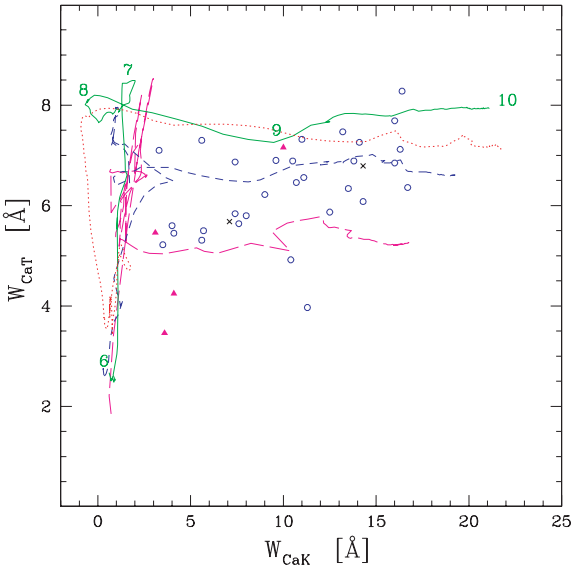

Figure 6. Same as Fig. 3 but without Seyfert 1 nuclei and overplotting simple stellar populations, as computed from the BC03 models. Lines are as in Fig. 5. Numbers in stellar lines denote log(Age[yr]). Symbols are as in Fig. 2.

Numbers along the model track mark ages of 10^6, 10^7, 10^8, 10^9 and 10^{10} yr. The first thing to note is that, unlike the bulge + FC mixing lines in Fig. 3, these models do span the region occupied by objects in our sample, showing that stellar populations alone are capable of explaining the behaviour of type 2 Seyfert galaxies in the CaK versus CaT diagram. Secondly, Fig. 6 seems to indicate that sub-solar abundances may be required to match the data on type 2 Seyfert galaxies, particularly those with weak CaT. This is somewhat surprising, given that we are dealing with the nuclei of early-type spirals, where Z is expected to be relatively high. One must nevertheless recall that these are SSP models, whereas actual galaxies contain a mixture of stellar populations. This is particularly true for type 2 Seyfert galaxies, where previous studies have revealed a wide variety of star formation histories (Cid Fernandes et al. 2001, 2004; Wild et al. 2007). More realistic star formation histories can be modelled as a mixture of SSP, whose effect on this diagram can be conceived drawing imaginary mixing lines connecting any series of points along the instantaneous burst tracks.

3.3 Mixed models: Young plus Old populations

To have a rough idea of the effects of such a mixture, in Fig. 7 we repeat the spectral mixing experiment of Fig. 3 but this time using a 1 Myr population (to represent ongoing star formation) instead of a non-stellar power-law continuum. Solar and 2.5 solar BC03 models are used. We further allow for the possibility that the young population suffers more extinction than the old one, so we consider three cases: $A_V = 0$, 1.5 and 3 mag. Again, we do not plot Seyfert 1 nuclei, as they present dilution due to the non-stellar continuum and thus are out of the scope of this experiment. This exercise is essentially the same as that performed with a power-law FC in Fig. 3, except that the continuum shape is not the same, and, due to contamination by Paschen lines, $W_{\rm CaT}$ is not = 0 for a pure starburst (see Fig. 5, middle panel).

As is evident in the figure, these mixing lines span the observed points for most of the Sy 2 sample. It is important to emphasize that

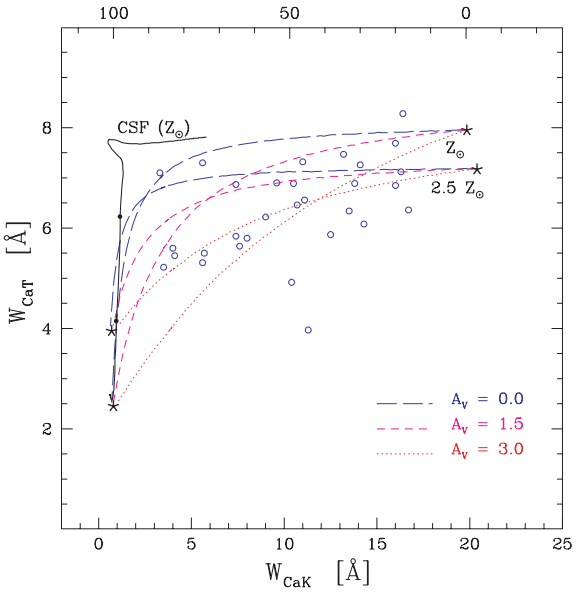

Figure 7. Same as Fig. 6 now overplotting old plus reddened young stellar population models for solar and 2.5 solar metallicity. Upper scale shows the percentage of the starburst contribution in the CaK region, $x^{\rm Stb}_{\rm CaK}$. Mixture lines correspond to different extinction magnitudes and the asterisks denote null (0 per cent, upper right) and full (100 per cent, lower left) young contribution. The CSF line refers to continuous star formation from ages between 1 Myr and 10 Gyr. Dots on this line indicate bursts of 5 and 10 Myr old.

only for very young populations one expects a relatively low CaT. As shown in the plot, galaxies with $W_{\rm CaT} < 6$ Å and $W_{\rm CaK} < 10$ Å require such a population to be adequately modelled. Not even the $0.4\,{\rm Z}_{\odot}$ models are capable of modelling these objects without a very young population.

It is also important to note that although our 1 Myr + 10 Gyr mixing models span most of the observed points in the CaK versus CaT plane, galaxies with $W_{\rm CaT}$ above ∼6 Å can be equally well modelled with an older young population. For metallicities $\geq 0.4\,{\rm Z}_{\odot}$, $W_{\rm CaT}$ rises above 6 Å as early as ∼5 Myr, with the appearance of the first RSGs. This also happens for continuous star formation models, as shown by the solid line in the CaT–CaK diagram.

Mixing models for ≥5 Myr + 10 Gyr populations are not shown for clarity, but, as can be deduced from Fig. 6, they would span most of the upper part of CaK versus CaT plane, where many Sy 2s are located. We note in passing that TDT originally suggested that the CaT in type 2 Seyfert galaxies signal the presence of RSG in a starburst. While this may well be true in some cases, our modelling shows that there is no way of telling it just from the strength of the CaT, since we are able to fit the $W_{\rm CaT}$ and $W_{\rm CaK}$ data both with and without RSGs.

Given the simplicity of these models, the overlap between data and models in the CaT–CaK diagram is highly encouraging. Nevertheless, at the middle of the diagram there are two Sy 2s that are far away from our models. The two 'outliers' are Mrk 3 and NGC 7212. It may be that a bona fide AGN continuum is present in these galaxies, which would help explaining their low CaK and specially CaT lines. The spectral synthesis analysis of NGC 7212 by Cid Fernandes et al. (2004) indicates that ∼35 per cent of the light at 4020 Å comes from an FC component. They also identify a weak broad Hβ, strengthening the case for the presence of a non-stellar continuum. Furthermore, for both NGC 7212 and Mrk 3, imaging (Pogge & De Robertis 1993; Kotilainen & Ward 1997), spectropolarimetery (Tran 1995) and spectral modelling (González Delgado et al. 2001) all point to the existence of an FC component (see Cid Fernandes et al. 2001 for a detailed discussion). None of these studies finds compelling evidence for significant on-going star formation in these galaxies. It is therefore likely that their low $W_{\rm CaT}$ values (the smallest amongst type 2 Seyfert galaxies) are indeed due to dilution by non-stellar light, explaining why they deviate from the region spanned by our purely stellar models in Fig. 7.

A consistent scenario thus emerges, where the blue continuum which dilutes the optical spectrum of some type 2 Seyfert galaxies is due to young stellar populations, while their undiluted CaT strengths can be explained as due to RSGs or older populations. As explained above, in the few cases where the CaT is low, a combination of an old plus a very young (pre-RSG) population is needed. In these cases, one may expect to see Paschen lines in absorption, which is not observed in our galaxies, as reported in Paper I.

To investigate this potential problem we have examined the strength of Paschen lines in the theoretical spectra of the mixing models shown in Fig. 7. We pay particular attention to the Pa14 line at 8598 Å, which is strategically placed between Ca2 and Ca3. We find that, for $A_V = 0$, Pa14 only becomes visible for $x^{\rm Stb}_{\rm CaK} >$ 95 per cent or 85 per cent for $Z = 1$ and $2.5\,{\rm Z}_{\odot}$, respectively. These fractions fall to about 75 per cent if we consider 3 mag of differential extinction. These very large fractions result from the fact that the young population is much bluer than the old one, so any mixture where young stars contribute significantly to the CaT range automatically implies that this same component completely dominates in the optical. Spectral synthesis studies in the optical range never find such huge starburst contribution in type 2 Seyfert galaxies. Thus, the non-detection of Paschen lines may be simply due to the fact that old stars dominate the flux in the near-IR, even when younger populations dominate the optical light.

A further factor which may be related to the non-detection of Paschen absorption is filling by an emission component, powered either by the AGN or by a circumnuclear starburst. A few of our galaxies do show a hint of Pa14 emission, like the starburst galaxy NGC 7714, where Pa14 has about 0.5 Å emission equivalent width (see also González Delgado et al. 1995). In other cases, emission and absorption may approximately compensate each other. This seems to be the case in the super star clusters of NGC 1569, where WR features, high-order Balmer absorption lines and the CaT, are all clearly detected (González Delgado et al. 1997), but Paschen lines are not seen either in absorption or in emission. Hence, even though further studies concerning Paschen lines are desirable, their no detection does not invalidate our conclusions.

4 CAT STRENGTH AS A FUNCTION OF DISTANCE TO THE NUCLEUS

All CaT data reported so far pertain to nuclear regions. For 34 of the 78 galaxies studied in Paper I, our long-slit data are of sufficient quality to warrant the extraction of spatially resolved spectra. Detailed results for all such sources are presented in Asari (2006). In this section, we summarize the main results concerning the spatial behaviour of the CaT strength.

Fig. 8 shows $W_{\rm CaT}$ spatial profiles for six galaxies, chosen to represent type 1 Seyfert galaxies (panels a and b), type 2 Seyfert galaxies (c and d) and composite starburst + Seyfert 2 (e and f). There is a clear drop in $W_{\rm CaT}$ as one approaches the nucleus in type 1 Seyfert galaxies, whereas type 2 Seyfert galaxies present remarkably flat $W_{\rm CaT}(r)$ profiles. At a few hundred pc from the nucleus, however, the CaT strength becomes similar for both Seyfert types.

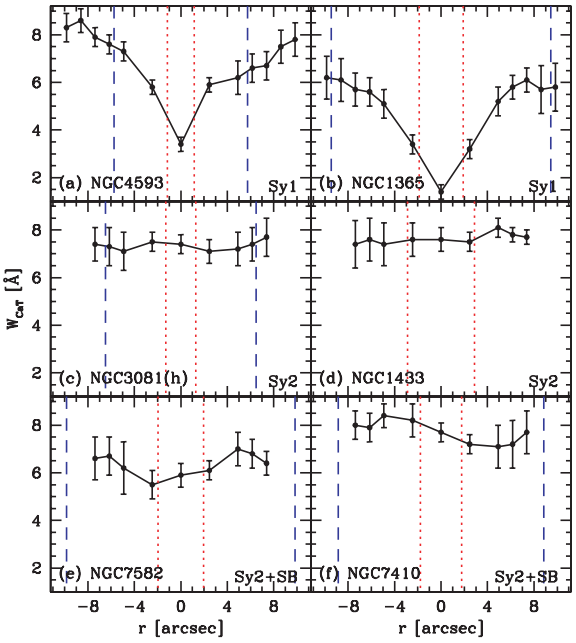

Figure 8. Examples of $W_{\rm CaT}$ spatial profiles. Dotted lines mark −200 to +200 pc region and dashed lines the −1 to +1 kpc region. Panels (a) and (b) show the dilution of $W_{\rm CaT}$ in Seyfert 1; panels (c)–(f) show how flat $W_{\rm CaT}$ is for type 2 Seyfert galaxy and type 2 Seyfert galaxy + starburst.

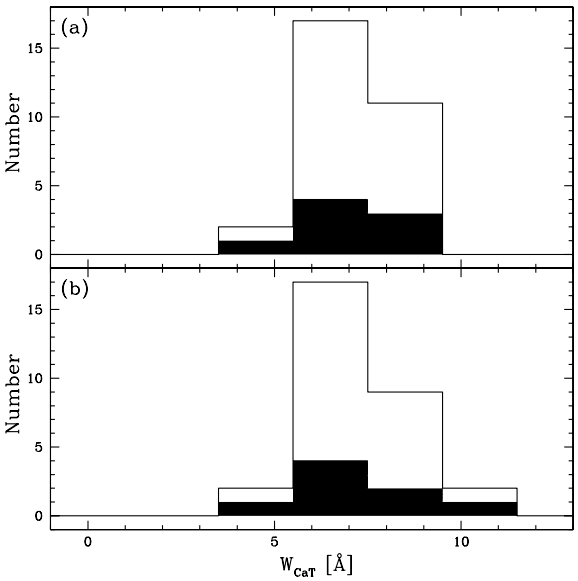

Figure 9. Similar to Fig. 1 but for off-nuclear measurements. (a) 1 kpc data and (b) furthest point for which we have signal (see text for details). Scale and areas are as in Fig 1.

Table 2. Statistics for spatial $W_{\rm CaT}$ measurements: minimum, median and maximum values are shown for type 1 and type 2 Seyfert galaxy and for nuclear and off-nuclear data. For off-nuclear data, we considered ≤1 kpc data, which refer to the values at 1 kpc or less from the nucleus, and *furthest* data, which are the corresponding values of furthest points from the nucleus of each galaxy for which we have signal.

	Nuclear (Å)	≤1 kpc (Å)	Furthest (Å)
Seyfert 1 – min	2.7	4.3	5.0
Seyfert 1 – med	4.8	6.5	6.6
Seyfert 1 – max	6.7	8.3	9.0
Seyfert 2 – min	4.0	3.9	3.7
Seyfert 2 – med	6.5	6.4	6.4
Seyfert 2 – max	8.3	8.3	9.1

This illustrates once again how sensitive $W_{\rm CaT}$ is to an underlying FC, in agreement with the results reported in Section 2.

In a way, these results are arguably more convincing proof of the FC effects. Since the analysis in Section 2 was based on a comparison of CaT strengths for type 1 and type 2 Seyfert galaxies, or with fiducial values, one could worry that for some reason the stellar populations of the two kinds of AGN are intrinsically different, invalidating a comparative analysis. Here, on the other hand, we show that at least immediately outside their nuclear regions, type 1 and type 2 Seyfert galaxies are very similar, and that dilution is really a nuclear effect present only in type 1 Seyfert galaxies. To further illustrate this, Fig. 9 repeats the comparison performed in Fig. 1, but this time using off-nuclear $W_{\rm CaT}$ measurements. Depending of the galaxy redshift, the furthest off-nuclear measurements correspond to less than 1 to ∼3 kpc. In Fig. 9(a), we proceed as follows. In the first cases (nearest galaxies), we take the furthest points from the nucleus (e.g. NGC 1433 in Fig. 8), and in the second cases (furthest galaxies), we first obtained the interpolated CaT values at exactly 1 kpc taking into account the data at each side of the nucleus, and then we calculate the average of the interpolated values (e.g. NGC 3081 in Fig. 8). We see that the differences between type 1 and type 2 Seyfert galaxies disappear when considering these off-nuclear values, which we call '≤1 kpc' data. Fig. 9(b) does the same thing, but using the values corresponding to the furthest points from the nucleus for which we have signal, and we call them '*furthest*' data. Numerical results of $W_{\rm CaT}$ spatial measurements are summarized in Table 2. A Kolmogorov-Smirov (KS) test applied to the distributions yields probabilities of $p = 0.46$ ('≤1 kpc') and $p = 0.84$ ('*furthest*'). We see that even for short distances (≤1 kpc), there is no significant dilution of CaT in type 1 Seyfert galaxies, as we expected from the regions outside the nuclei.

It is also interesting to point out that these results are essentially identical to those obtained from the spatial analysis of the CaK strength by Cid Fernandes et al. (1998) and Storchi-Bergmann et al. (1998, their fig. 1). Hence, the FC which dilutes the optical spectrum in type 1 Seyfert galaxies is the same which decreases the CaT strength in the near-IR. This component is not present in Kolmogorov-Smirov (KS).

The behaviour of $W_{\rm CaT}(r)$ for starburst + type 2 Seyfert galaxy composites (Figs 8e and f), on the other hand, contrasts with that derived from $W_{\rm CaK}$ radial profiles. Contrary to the strong spatial dilution by young stars detected in the CaK and other optical lines, the CaT profiles show very little, if any, variation as a function of distance to the nucleus in composite systems. In NGC 7582, there is a marginal hint of dilution. From optical work, we know that this galaxy hosts a very dusty central starburst, so it could represent a case where the starburst light does contribute to the flux in the CaT range with a non-negligible fraction. However, even in this most favourable case the nuclear CaT is diluted by less than 15 per cent with respect to its value at $r \sim \pm 500$ pc. In contrast, the optical absorption lines are much more diluted. At the wavelengths of the CaK, *G* band and MgIb lines, the dilution factors are 70, 60 and 57 per cent, respectively. To better appreciate this strong difference, we invite the reader to compare Fig. 8(e) with fig. 29 of Cid Fernandes et al. (1998), where the radial profiles of several optical absorption lines in NGC 7582 are shown.

The difference in $W_{\rm CaT}$ and $W_{\rm CaK}$ profiles is striking, but not surprising. In fact, our finding that the CaT does not mimic the CaK

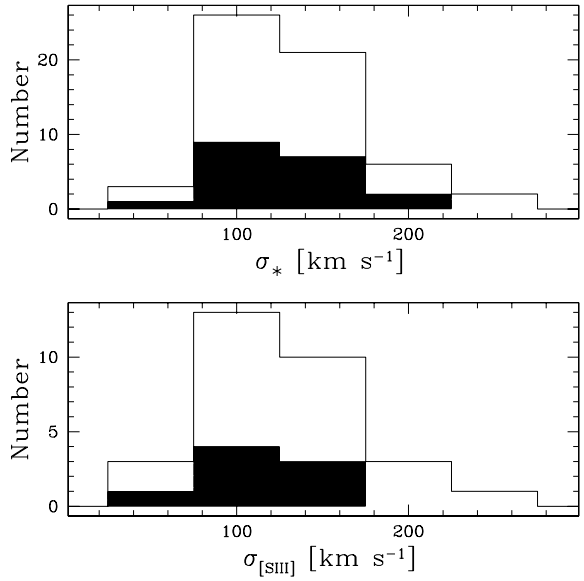

Figure 10. Distributions of stellar velocity dispersions ($\sigma_\star$, top) and [S III]-based gas velocity dispersions ($\sigma_{[S\,III]}$, bottom). Areas as explained in Fig. 1.

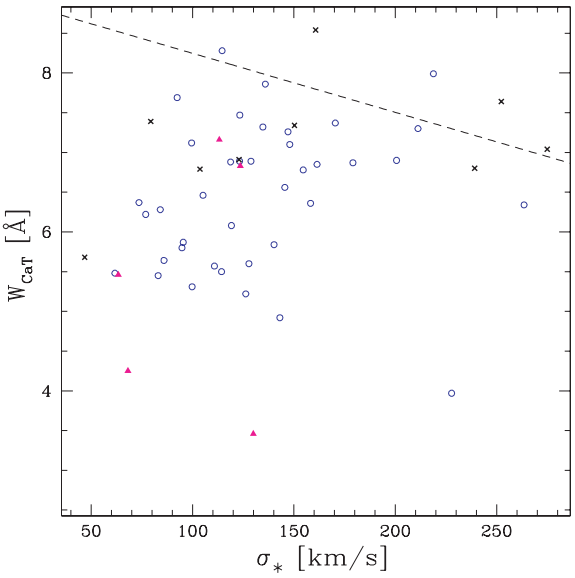

Figure 11. CaT values versus stellar velocity dispersions. Dashed line represents Saglia's fit (see text). Symbols are as in Fig. 2.

spatial behaviour is fully consistent with the conclusion laid out in the above section that only under extreme conditions (very young age and large extinction) would a starburst strongly dilute both CaK and CaT lines.

5 KINEMATICS

Our spectroscopic data (Paper I) provide estimates of two characteristic velocities: the typical velocity of stars through the host's bulge, $\sigma_\star$, and the typical NLR cloud velocity dispersions, inferred from the width of the [S III]λ9069 line. We fitted the profile of [S III]λ9069 with one or two Gaussians, one representing the core of the emission line and the other, if necessary, representing the wings. The resulting full width at half-maximum (FWHM) of the core component divided by $(8\ln 2)^{1/2}$ is what we call $\sigma_{[S\,III]}$. We have determined $\sigma_{[S\,III]}$ by this method for 31 Seyfert and four starburst nuclei.

The distributions obtained for $\sigma_\star$ and $\sigma_{[S\,III]}$ are shown in Fig. 10. They show that both types of nuclei have essentially the same (statistical) values: for Seyfert 1s $\sigma_\star = 128 \pm 37\,\mathrm{km\,s^{-1}}$ and $\sigma_{[S\,III]} = 111 \pm 29\,\mathrm{km\,s^{-1}}$, while for type 2 Seyfert galaxies $\sigma_\star = 134 \pm 45\,\mathrm{km\,s^{-1}}$ and $\sigma_{[S\,III]} = 137 \pm 76\,\mathrm{km\,s^{-1}}$. First, we will discuss the stellar velocity dispersions ($\sigma_\star$) and then we will analyse the NLR kinematics through $\sigma_{[S\,III]}$ and its possible link to $\sigma_\star$.

5.1 $\sigma_\star$ versus W_{CaT}

As reviewed in Section 1, recent work on normal galaxies has dedicated much attention to the fact that W_{CaT} is slightly anti-correlated with velocity dispersion all the way from dwarf to giant elliptical galaxies and bulges (Saglia et al. 2002; Cenarro et al. 2003; Falcón-Barroso et al. 2003; Michielsen et al. 2003). Even though our CaT data are not of the same quality as that employed in these studies, it is interesting to check whether starburst and active galaxies follow the same W_{CaT}–$\sigma_\star$ as normal ones.

Fig. 11 shows the results of this test. Clearly, as a whole, our galaxies do not follow a well-defined W_{CaT}–$\sigma_\star$ relation at all. The few normal galaxies in our sample (crosses), as well as the high-$\sigma_\star$ type 2 Seyfert galaxies, do tend to follow a similar anti-correlation found by Saglia et al. (2002) for ellipticals. However, there is a large population of galaxies with low $\sigma_\star$ and relatively low W_{CaT} which has no correspondence in previous studies of this relation. Excluding Mrk 3 and NGC 7212 (which are diluted by FC, as discussed in Section 3.3), the most deviant points are the starbursts NGC 1140, NGC 3256 and NGC 7714, located in the bottom left part of the plot. Next, at W_{CaT} between 5 and 6.5 Å and $\sigma_\star < 150\,\mathrm{km\,s^{-1}}$ are the composite starburst–type 2 Seyfert galaxies nuclei, like NGC 5135, NGC 7582, IC 3639, Mark 1. It thus seems that the complex star formation histories of these objects are somehow related to their displacement with respect to the W_{CaT}–$\sigma_\star$ relation defined for more well-behaved systems. Interestingly, the normal galaxy NGC 205 is located away from the anti-correlation stated for normal nuclei. This dwarf elliptical galaxy has a low metallicity (Mateo 1998), which indicates that it could also influence the CaT–$\sigma_\star$ relation.

5.2 Stellar versus NLR kinematics

The question concerning the acceleration of gas in the NLR has been analysed in several papers (NW; TDT). As pointed out by Greene & Ho (2005, hereafter GH), the NLR is small enough to be illuminated by the active nucleus and large enough to feel the gravitational forces of the bulge of the host galaxy. Comparison between gas and stellar kinematics was previously carried out by NW using the [O III]λ5007 line, who find that $\sigma_\star$ and the FWHM of [O III]λ5007 are correlated, but with substantial scatter. Recent work on type 1 Seyfert galaxies (Jiménez-Benito et al. 2000) and Sloan Digital Sky Survey galaxies (Heckman et al. 2004; GH) confirms this finding. The implication is that the NLR clouds are at least partly dominated by virial motions in the host galaxy's bulge. Given the existence of this relation, forbidden linewidths have sometimes been used as a surrogate for $\sigma_\star$ in the absence of information on the stellar dynamics (Nelson 2000; Grupe & Mathur 2004). The case of narrow-line Seyfert 1 (NLS1) galaxies is particularly interesting. In a recent paper, Komossa & Xu (2007) have shown that, for these Seyfert galaxies, $\sigma_{[O\,III]}$ can be used as a proxy for $\sigma_\star$ only after removing the (usually blue) wings of the [O III] profile. In

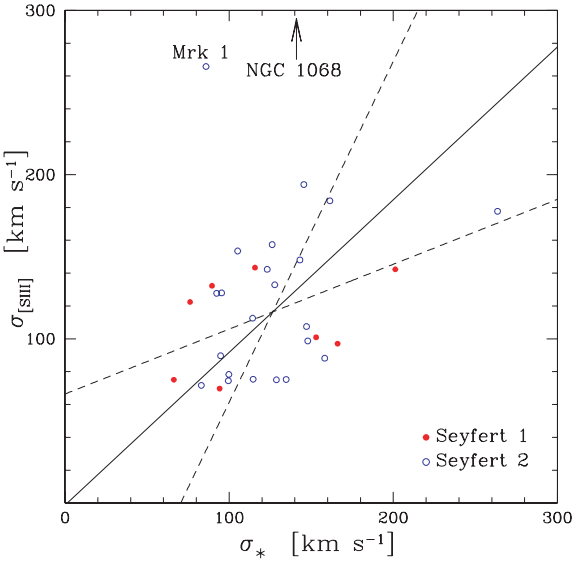

Figure 12. Comparison of stellar velocity dispersions with our estimate of $\sigma_{\rm gas}$ based on the width of the [S III]λ9069 line. Symbols are as in Fig. 2. OLSs regressions are applied over all data but Mrk 1 and NGC 1068: solid, OLS Bisector fit; dashed, OLS $(X|Y)$ and OLS $(Y|X)$ (shallowest and steepest lines, respectively).

other words, $\sigma_{[\rm O\,III]}$ should correspond only to the core of the line, similarly to what we have done in the present paper in the fit of the [S III] emission-line profiles to obtain $\sigma_{[\rm S\,III]}$.

In Fig. 12, we compare our values of $\sigma_{[\rm S\,III]}$ and $\sigma_\star$ for all Seyfert nuclei. We note that two of them, namely Mrk 1 and NGC 1068, have $\sigma_{[\rm S\,III]}$ much larger than $\sigma_\star$. Evidence of jets was found in these galaxies, which may explain the acceleration of the gas via shocks produced in the interaction within jets and NLR. Excluding these two nuclei, we have fitted all the other galaxies by linear relations given by Ordinary Least Square (OLS) regressions (Isobe et al. 1990). Solid line represents the OLS Bisector fit, while dashed lines are OLS $(X|Y)$ and OLS $(Y|X)$ (shallowest and steepest lines, respectively). The OLS Bisector fit gives a slope of 0.93 ($N = 29$, $R_S = 0.37, P = 0.046$). Taking into account just type 2 Seyfert galaxies, we find a slope of 1.03 ($N = 21, R_S \sim 0.40, P = 0.07$) and 0.73 for type 1 Seyfert galaxies, for which there is not a clear correlation ($R_S \sim 0.31, P = 0.45$). The slopes and correlation coefficients do not vary substantially when we exclude worst quality data. Using the a = very good, b = good and c = not-too-bad quality flags adopted in Paper I, we find for $a + b$ a slope of 1.00 ($N = 23, R_S = 0.39, P = 0.06$) and 1.00 for a sources alone ($N = 20, R_S = 0.3, P = 0.2$). All these are summarized in Table 3. Interestingly, there is also a tendency for four starburst nuclei, with a slope of about 0.56 and $R_S \sim 0.81$ (not shown here).

We repeated this analysis using $\sigma_{[\rm O\,III]} = {\rm FWHM}_{[\rm O\,III]}/(8\ln 2)^{1/2}$ taken from the literature (Whittle 1992; Bassani et al. 1999; Schmitt et al. 2003). NGC 1068, Mrk 1 and Mrk 78 present very different values of $\sigma_{[\rm O\,III]}$ and $\sigma_\star$. Further excluding the worst quality data ('flag *c*' in Whittle 1992 and our flag *d*), the OLS Bisector fit gives a slope of 1.48 ($R_S = 0.42$) for the whole sample (28 objects), while splitting into type 1 and type 2 Seyfert galaxies the slopes are 1.13 ($R_S = 0.81$) and 1.60 ($R_S = 0.33$), respectively. This is described in Table 4. We point out that for this analysis we used FWHM data of [O III] line, which are (in median) larger than our estimates of $\sigma_{\rm gas}$ through the FWHM of the *core* of [S III] line, so that the slope of a fit applied to [O III] data yields larger values than those obtained for [S III] data. We confirm this fitting $\sigma_{[\rm S\,III]}$ versus $\sigma_{[\rm O\,III]}$, which gives a slope of ∼0.85 (R_S ∼0.44, 20 objects).

Table 3. Results of OLS Bisector fits for $\sigma_{[\rm S\,III]} - \sigma_\star$. Letters in Columns 5 and 6 denote the quality flags (see text).

	All	Sy 1	Sy 2	All $(a+b)$	All (a)
Slope	0.93	0.73	1.03	1.00	1.00
N	29	8	21	23	20
R_S	0.37	0.31	0.40	0.39	0.30
P	0.046	0.45	0.07	0.06	0.20

Table 4. Results of OLS Bisector fits for $\sigma_{[\rm O\,III]} - \sigma_\star$.

	All	Sy 1	Sy 2
Slope	1.48	1.13	1.60
N	28	12	16
R_S	0.42	0.81	0.33

There are, therefore, correlations between NLR and stellar motions, but with considerable scatter. One way to study this scatter is to look at the residuals $\sigma_{[\rm S\,III]}/\sigma_\star$ about unity. Fig. 13 shows this distribution, which is a moderately peaked (kurtosis ~ -1) Gaussian for the majority of type 2 Seyfert galaxies. Without taking into account the two galaxies with abnormally high gaseous velocity dispersion (for which it was shown that there are several kinematical components), $\sigma_{[\rm S\,III]}/\sigma_\star = 0.97 \pm 0.32$ (average and rms dispersion), while for type 1 and type 2 Seyfert galaxies $\sigma_{[\rm S\,III]}/\sigma_\star$ are 1.02 ± 0.40 and 0.95 ± 0.29, respectively, i.e. $\sigma_{[\rm S\,III]}/\sigma_\star$ is the same for both types of objects. Fig. 13 is similar to Fig. 7 of NW, which uses [O III]-based gas kinematics. Although NW have twice as many objects, we note that our distribution is more concentrated around unity, mainly because we have FWHM determinations of Gaussians fitted to the *core* of the [S III] line.

All this study shows that the [S III] core emitting zone of the NLR is dynamically linked to the gravitational bulge potential, a result similar to that obtained by Komossa & Xu (2007) for NLS1 galaxies.

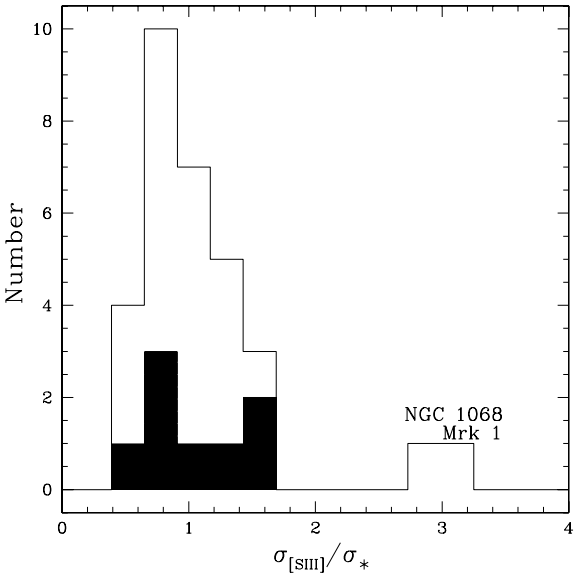

Figure 13. Distribution of gas to stellar velocity dispersions ratio, $\sigma_{[\rm S\,III]}/\sigma_\star$. Areas as explained in Fig. 1.

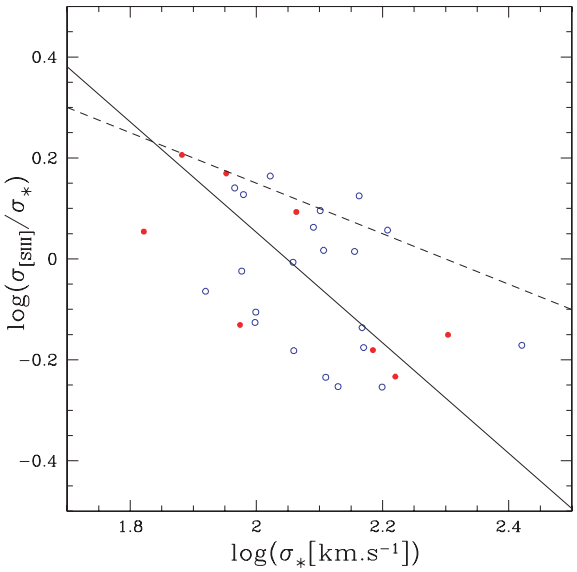

Figure 14. Deviation from $\sigma_{[S\,III]}/\sigma_\star$ with $\sigma_\star$. Solid line is the least-squares fit for all Seyfert galaxies. Dotted line, Green & Ho's fit. Symbols are as in Fig. 2.

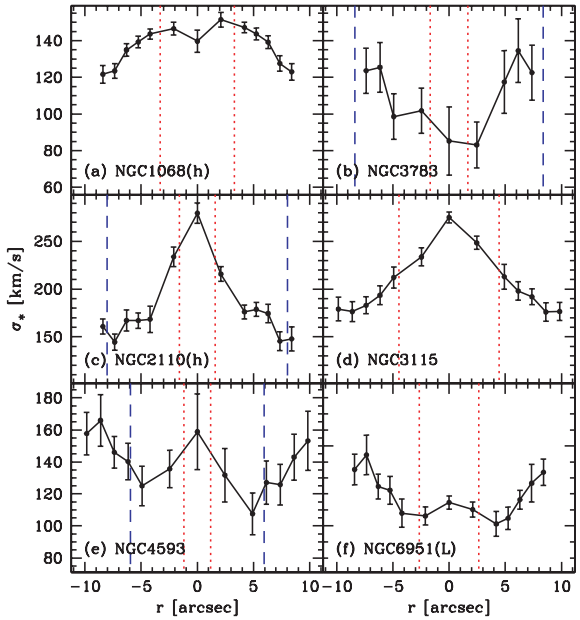

Figure 15. Examples of $\sigma_\star$ spatial variations. Dotted lines mark −200 to +200 pc region; dashed lines, the −1 to +1 kpc region.

However, we see that there are possible secondary factors besides gravitational potential that could explain the scatter about unity in NLR kinematics. Shocks and other acceleration mechanisms could account for the high-velocity clouds observed in a few galaxies, but in general a complete study of gas stellar kinematics remains to be done.

A detailed analysis of stellar and gaseous kinematics of NLR was made by GH taking precisely $\sigma_{[S\,III]}/\sigma_\star$ as the central quantity of their study. They found that none but one of the nuclear activity indicators is correlated with $\sigma_{[S\,III]}/\sigma_\star$; only with $\log\sigma_\star$, which is indirectly a measure of bulge mass, there is a hint of relationship. Although we have few points, we note this trend in our data, which is shown in Fig. 14 together with GH's best fit. Again, applying OLS Bisector fit, we obtain $\log\sigma_{[S\,III]}/\sigma_\star = -1.1\,\log\sigma_\star + 2.2$, with $R_S = -0.55$. A least-squares fit gives $\log\sigma_{[S\,III]}/\sigma_\star = -0.56\,\log\sigma_\star + 1.13$ ($R_S = -0.55, P = 0.022$), nearly the same relation obtained by them. Only for type 2 Seyfert galaxies there is a weaker (but real) trend, $\log\sigma_{[S\,III]}/\sigma_\star = -0.41\,\log\sigma_\star + 0.81$ ($N = 21, R_S = -0.37, P = 0.09$), while for Seyfert 1s the correlation is moderately strong, $\log\sigma_{[S\,III]}/\sigma_\star = -0.74\,\log\sigma_\star + 1.50$ ($N = 8, R_S = 0.75$, $P = 0.036$).

We checked whether $\sigma_{[S\,III]}/\sigma_\star$ correlates with other properties, like morphological and activity types, redshift, inclination, etc., but (like GH) found no strong trend. The absence of a trend with the inclination of the host galaxy suggests that the gas in the NLR has random velocities and so the velocity field is similar to that of the stars, as previously found by NW (their fig. 11).

Our data thus support the existence of an anti-correlation between $\sigma_{[S\,III]}$ and $\sigma_\star$, albeit with a large scatter. Using $\sigma_{[S\,III]}$ as a proxy of $\sigma_\star$ tends to underestimate velocity dispersion in bulge of massive galaxies. In any case, given the existence of a correlation between both (gas and stellar) velocity dispersions, and taking into account that [S III] is a high ionization line produced very near the active nucleus and often with strong wings like [O III], our study supports the idea of using $\sigma_{[S\,III]}$ as a kinematic tracer of the NLR.

5.3 Spatially resolved kinematics

As an extension of our spatial analysis, we report results for the variations in kinematical properties of our sub-sample.

Fig. 15 shows examples of spatial variations in $\sigma_\star$. Some recent works (García-Lorenzo, Mediavilla & Arribas 1999; Emsellem et al. 2001; Márquez et al. 2003; Barbosa et al. 2006) have discussed the possibility of a *sigma-drop* detection, i.e. $\sigma_\star$ is appreciably lower towards nuclear regions due to the presence of a star-forming cold nuclear disc. We see a nuclear drop in $\sigma_\star$ in only two galaxies (Fig. 15a and b). For some objects, there is even a hint of a rise in $\sigma_\star$ in their central parts (e.g. Fig. 15c and d). We have to keep in mind, however, that our spectra do not have the spatial resolution needed to detect this behaviour in $\sigma_\star$, which would require a resolution of a few tens parsecs.

Another interesting feature that can be seen for some of our objects is a symmetric off-nuclear drop in $\sigma_\star$, as in NGC 4593 (Fig. 15e). This is in agreement with the detailed integral field spectroscopy of this object made by Barbosa et al. (2006), who found a partial ring of low $\sigma_\star$ nearly at the same distance from the nucleus. A similar behaviour is seen in NGC 6951 (Fig. 15f). *U*-band images of these galaxies (Muñoz Marín et al. 2007) show the presence of young stars at the locations where the off nuclear $\sigma_\star$ drops are observed.

6 SUMMARY

In Paper I, we presented a spectroscopic atlas of 78 galaxies in the region of CaT lines, and measured the equivalent widths of CaT and [S III]λ9069 lines, and stellar and gaseous velocity dispersions. In this paper, we used these data, as other measurements, to investigate the CaT strength and the kinematical properties of Seyfert nuclei.

Our conclusions can be summarized as follows.

(i) The equivalent widths of CaT and [S III] are diluted in Seyfert 1s, due to the presence of a non-stellar component, while in type 2 Seyfert galaxies there is no sign of dilution. We show that the

nuclear dilution of CaT lines in type 1 Seyfert galaxies and the non-observed dilution in type 2 Seyfert galaxies hold spatially, i.e. within approximately the central kpc. At this distance, the effects disappear, thus implying that the stellar lines are diluted due the nuclear non-stellar continuum directly seen in type 1 Seyfert galaxies.

(ii) The CaT strength turns out not to be a good tracer for the mean ages and metallicities of metal-rich stellar populations. None the less, its combination with CaK line yields a useful constraint on the nature of the continuum emission from optical to near-IR wavelengths.

(iii) We show that the location of type 2 Seyfert galaxies in the CaT–CaK plane could be explained satisfactorily by stellar population synthesis models, by considering mixtures of an old plus very young stellar populations with an extinction of just two or three magnitudes. The hypothesis of Seyfert 2 nuclei composition as a mixing of an old stellar population plus power-law central source cannot account for the majority of the data.

(iv) There is a correlation between nuclear $\sigma_\star$ and $\sigma_{[\mathrm{S\,III}]}$, as well as an anti-correlation between $\sigma_{[\mathrm{S\,III}]}/\sigma_\star$ and $\sigma_\star$, both with a substantial scatter. This means that care must be exercised when using $\sigma_{[\mathrm{S\,III}]}$ as a proxy for $\sigma_\star$. These results are compatible with previous results of NW and GH.

ACKNOWLEDGMENTS

LRV, NVA, RCF, AGR and TSB acknowledge the support of Capes and CNPq. LRV acknowledges the support from Secyt and the hospitality of UFSC. RGD acknowledges support by Spanish Ministry of Science and Technology (MCYT) through grant AYA-2001-3939-C03-01. We thank Laboratório Nacional de Astrofísica for the allocation of time on ESO 1.52 m and financial support during the runs. We also thank the referee, Javier Cenarro, for the very useful comments which greatly improved the content of the paper. A part of the data described here was taken at Kitt Peak National Observatory, National Optical Astronomy Observatories, which are operated by AURA, Inc., under a cooperative agreement with the National Science Foundation. Basic research at the NRL is supported by 6.1 base funding. This research made use of the NASA/IPAC Extragalactic Data base (NED), which is operated by the Jet Propulsion Laboratory, Caltech, under contract with NASA.

REFERENCES

Antonucci R., 1993, ARA&A, 31, 473
Armandroff T. E., Zinn R., 1988, AJ, 96, 92
Asari N. V., 2006, Dissertac̆ao de Mestrado. Universidade Federal de Santa Catarina, Brazil
Barbosa F. K. B., Storchi-Bergmann T., Cid Fernandes R., Winge C., Schmitt H., 2006, MNRAS, 371, 170
Bassani L., Dadina M., Maiolino R., Salvati M., Risaliti G., della Ceca R., Matt G., Zamorani G., 1999, ApJS, 121, 473
Botte V., Ciroi S., Rafanelli P., Di Mille F., 2004, AJ, 127, 3168
Bruzual G., Charlot S., 2003, MNRAS, 344, 1000 (BC03)
Cenarro A. J., Cardiel N., Gorgas J., Peletier R. F., Vazdekis A., Prada F., 2001a, MNRAS, 326, 959
Cenarro A. J., Gorgas J., Cardiel N., Pedraz S., Peletier R. F., Vazdekis A., 2001b, MNRAS, 326, 981
Cenarro A. J., Gorgas J., Cardiel N., Vazdekis A., Peletier R. F., 2002, MNRAS, 329, 863
Cenarro A. J., Gorgas J., Vazdekis A., Cardiel N., Peletier R. F., 2003, MNRAS, 339, L12
Cenarro A. J., Sánchez-Blázquez P., Cardiel N., Gorgas J., 2004, ApJ, 614, L101
Chabrier G., 2003, PASP, 115, 763
Cid Fernandes R., Terlevich R., 1995, MNRAS, 272, 423
Cid Fernandes R., Storchi-Bergmann T., Schmitt H., 1998, MNRAS, 297, 579
Cid Fernandes R., Heckman T., Schmitt H., González Delgado R. M., Storchi-Bergmann T., 2001, ApJ, 558, 81
Cid Fernandes R., Gu Q., Melnick J., Terlevich E., Terlevich R., Kunth D., Rodrigues Lacerda R., Joguet B., 2004, MNRAS, 355, 273
Díaz A. I., Terlevich E., Terlevich R., 1989, MNRAS, 239, 325
Emsellem E., Greusard D., Combes F., Friedli D., Leon S., Pécontal E., Wozniak H., 2001, A&A, 368, 52
Falcón-Barroso J., Peletier R. F., Vazdekis A., Balcells M., 2003, ApJ, 588, L17
García-Lorenzo B., Mediavilla E., Arribas S., 1999, ApJ, 518, 190
García-Vargas M. L., Molla M., Bressan A., 1998, A&AS, 130, 513
Garcia-Rissmann A., Vega L. R., Asari N. V., Cid Fernandes R., Schmitt H., González Delgado R. M., Storchi-Bergmann T., 2005, MNRAS, 359, 765 (Paper I)
González Delgado R. M., Perez E., Diaz A. I., García-Vargas M. L., Terlevich E., Vilchez J. M., 1995, ApJ, 439, 604
González Delgado R. M., Leitherer C., Heckman T., Cervio M., 1997, ApJ, 483, 705
González Delgado R. M., Heckman T., Leitherer C., 2001, ApJ, 546, 845
Greene J. E., Ho L. C., 2005, ApJ, 627, 721 (GH)
Grupe D., Mathur S., 2004, ApJ, 606, L41
Heckman T. M., Kauffmann G., Brinchmann J., Charlot S., Tremonti C., White S. D. M., 2004, ApJ, 613, 109
Idiart T. P., Thevenin F., de Freitas Pacheco J. A., 1997, AJ, 113, 1066
Isobe T., Feigelson E. D., Akritas M. G., Babu G. J., 1990, ApJ, 364, 104
Jiménez-Benito L., Díaz A. I., Terlevich R., Terlevich E., 2000, MNRAS, 317, 907
Komossa S., Xu D., 2007, ApJ, 667, 33
Koski A. T., 1978, ApJ, 223, 56
Kotilainen J. K., Ward M. J., 1997, A&AS, 121, 77
Le Borgne, J.-F. et al., 2003, A&A, 402, 433
Márquez I., Masegosa J., Durret F., González Delgado R., Moles M., Maza J., Pérez E., Roth M., 2003, A&A, 409, 459
Mateo M. L., 1998, ARA&A, 36, 435
Mayya Y. D., 1997, ApJ, 482, L149
Michielsen D., De Rijcke S., Dejonghe H., Zeilinger W. W., Hau G. K. T., 2003, ApJ, 597, L21
Michielsen D. et al., 2007, ApJ, 670, L101
Muñoz Marín V. M., González Delgado R., Schmitt H., Cid Fernandes R., Pérez E., Storchi-Bergmann T., Heckman T., Leitherer C., 2007, AJ, 134, 648
Nelson C. H., 2000, ApJ, 544, L91
Nelson C. H., Whittle M., 1996, ApJ, 465, 96 (NW)
Pogge R. W., De Robertis M. M., 1993, ApJ, 404, 563
Saglia R. P., Maraston C., Thomas D., Bender R., Colless M., 2002, ApJ, 579, L13
Schmitt H. R., Donley J. L., Antonucci R. R. J., Hutchings J. B., Kinney A. L., 2003, ApJS, 148, 327
Storchi-Bergmann T., Cid Fernandes R., Schmitt H. R., 1998, ApJ, 501, 94
Storchi-Bergmann T., Raimann D., Bica L., Fraquelli H., 2000, ApJ, 544, 747
Terlevich R., Davies R. L., Faber S. M., Burstein D., 1981, MNRAS, 196, 381
Terlevich E., Díaz A., Terlevich R., 1990, MNRAS, 242, 271 (TDT)
Tran H. D., 1995, ApJ, 440, 597
Tremaine S. et al., 2002, ApJ, 574, 740
Vazdekis A., Cenarro A. J., Gorgas J., Cardiel N., Peletier R. F., 2003, MNRAS, 340, 1317
Whittle M., 1992, ApJS, 79, 49
Wild V., Kauffmann G., Heckman T., Charlot S., Lemson G., Brinchmann J., Reichard T., Pasquali A., 2007, MNRAS, 381, 543

This paper has been typeset from a TEX/LATEX file prepared by the author.